Preparation and Characterization of Intercalation Compounds of Layered Double Hydroxides with Metallic Oxalato Complexes

Philippe Beaudot, Marie Elisabeth De Roy,* and Jean Pierre Besse

Laboratoire des Matériaux Inorganiques, Université Blaise Pascal, UMR CNRS 6002, 63177 Aubière Cedex, France

Intercalation of metallic oxalato complexes $CoOx_2^{2-}$, $CuOx_2^{2-}$, $MnOx_3^{3-}$, and $GaOx_3^{3-}$ in [Zn_2Al] and [Mg_2Al] LDHs was successfully carried out leading to well characterized products in which metallic complexes lying between layers were subjected to minor modifications following intercalation as confirmed by XRD, FTIR, and particularly XAFS studies. The obtained data permitted modeling the layout of metallic oxalato complexes between the layers for each compound. Thermal treatments undertaken on exchanged compounds led to a mixing of oxides with increase in surface areas particularly for the Ga-containing product. Dispersed oxide and metallic particules were obtained by a soft chemistry treatment in refluxing ethylene glycol.

1. Introduction

Layered double hydroxide (LDH) materials are the result of a combination of host net obtained by the stacking of inorganic layers and chemical species trapped in the interlamellar domain. The structure looks like a brucite type with a 2D distribution of coplanar octaedra [$M(OH)_6$] which corresponds to the hydrolyzed layer $M(OH)_2$ of the brucite.

The simultaneous presence of divalent and trivalent metallic cations in these layers leads to a positive charge which is balanced by anionic species located in the interlamellar space with water molecules. The ratio between divalent and trivalent metallic cations must be such that $M^{III}/(M^{II} + M^{III})$ value is from 0.2 to 0.4 for the majority of couples (M^{II}/M^{III}).[1] The general formula of LDH compounds is then [$M^{II}_{(1-x)}M^{III}_{(x)}(OH)_2$] [$X^{m-}_{x/m} \cdot nH_2O$].

According to the fields of application, a great choice of metallic couples (M^{II}/M^{III}) or interlayer species is possible. A main property of these materials is their anionic exchange capacity which makes them unique inorganic materials for intercalate organic or inorganic anions. It permits the use of LDH in several disciplines, such as medicine, environment, and, of course, catalysis.[2−4] The purpose of this work is to replace anionic species such as Cl^-, NO_3^-, etc., generally present in the interlamellar space, by metallic complexes[5] to obtain catalyst precursors. It is important to point out that papers have already dealt with the subject, which shows the interest of such compounds in heterogeneous catalysis.[6,28−35] The ultimate aim is to prepare a mixture of dispersed oxides

* To whom correspondence should be addressed. Marie.de_Roy@univ-bpclermont.fr.

(1) Miyata, S. *Clays Clay Miner.* **1980**, *28*, 50.
(2) de Roy, A.; Forano, C.; el Malki, K.; Besse, J. P. *Anionic Clays: Trends in Pillaring Chemistry*; Ocelli, Robson, Eds.; Van Nostrand Reinhold: New York, 1992; Vol. II, Chapter 7, p 108.
(3) Vaccari, A. *Appl. Clay Sci.* **1999**, *14*, 161.
(4) Rousselot, I.; Taviot-Guého, C.; Besse, J. P. *Int. J. Inorg. Mater.* **1999**, *1*, 165.
(5) Rives, V.; Ulibarri, M. A. *Coord. Chem. Rev.* **1999**, *181*, 61.

(6) Cavani, F.; Trifiro, F.; Vaccari, A. *Catal. Today* **1991**, *11*, 173.
(7) Hedge, M. S.; Larcher, D.; Dupont, L.; Beaudoin, B.; Tarascon, J. M. *Solid State Ionics* **1997**, *93*, 33.
(8) Kooli, F.; Rives, V.; Jones, W. *Chem. Mater.* **1997**, *9*, 2231.
(9) Freemantle, M. *Chem. Eng. News* **1998**, October 12, 40.
(10) Malyala, R. V.; Rode, C. V.; Arai, M.; Hedge, S. G.; Chaudhari, R. V. *Appl. Catal., A* **2000**, *193*, 71.
(11) Prévot, V.; Forano, C.; Besse, J. P. *J. Solid State Chem.* **2000**, *153*, 301.
(12) Carlino, S.; Hudson, M. J. *Solid State Ionics* **1998**, *110*, 153.
(13) Strobbe, E. R.; de Boer, B. A.; Geus, J. W. *Catal. Today* **1999**, *47*, 161.
(14) Wang, X.; Xie, Y.-C. *React. Kinet. Catal. Lett.* **2000**, *71*, 3.
(15) Sinka, A. S. K.; Shankar, V. *Chem. Eng. J.* **1993**, *52*, 115.
(16)) Donia, A. M.; Radwan, N. R. E.; Atia, A. A. *J. Therm. Anal. Calorim.* **2000**, *61*, 249.
(17) Artizzu, P.; Garbowski, E.; Primet, M.; Brulle, Y.; Just, J. S. *Catal. Today* **1999**, *47*, 83.
(18) Thomas, D. J.; Wehrli, J. T.; Wainwright, M. S.; Trimm, D. L.; Cant, N. W. *Appl. Catal., A* **1992**, *86*, 101.
(19) Chernavskii, P. A.; Pankina, G. V.; Lunin, V. V. *Catal. Lett.* **2000**, *66*, 121.
(20) Valente, A.; Bothelho do Rego, A. M.; Reis, I M. J.; Silva, F.; Ramos, A. M.; Vital, J. *Appl. Catal., A* **2001**, *207*, 221.
(21) Choudhary, V. R.; Mantri, K.; Jana, S. K. *Microporous Mesoporous Mater.* **2001**, *47*, 179.
(22) Derouane, E. G.; Abdul Hamid, II.; Ivanova, S. B.; Blom, N.; Holjund Nielsen, P. E. *J. Mol. Catal.* **1994**, *86*, 371.
(23) Dooley, K. M.; Price, G. L.; Kanazirev, V. I.; Hart, V. I. *Catal. Today* **1996**, *31*, 305.
(24) Giannetto, G.; Monque R.; Galiasso, R. *Catal. Rev.-Sci. Eng.* **1994**, *36*, 271.
(25) Halàsz, J.; Konya, Z.; Fudala, A.; Beres, A.; Kirisci, I. *Catal. Today* **1996**, *31*, 293.
(26) Arends, I. W. C. E.; Sheldon, R. A. *Appl. Catal., A* **2001**, *212*, 175.
(27) Miyata, S. *Clays Clay Miner.* **1983**, *31*, 305.
(28) Corma, A.; Fornés, V.; Rey, F. *J. Catal.* **1994**, *148*, 205.
(29) Natsuka, T.; Kawasaki, H.; Yamashita, S.; Kohjiya, S. *Bull. Chem. Soc. Jpn.* **1979**, *52*, 2449.
(30) Das, J.; Parida, K. *React. Kinet. Catal. Lett.* **2000**, *69*, 223.
(31) Watanabe, Y.; Tatsumi, T. *Microporous Mesoporous Mater.* **1998**, *22*, 399.
(32) Sychev, M.; Pridod'ko, R.; Erdman, K.; Mangel A.; van Santen, R. A. *Appl. Clay Sci.* **2001**, *18*, 103.
(33) Kanada, K.; Ueno, S.; Imakoa, T. *J. Chem. Soc., Chem. Commun.* **1994**, 797.

which present activities in catalysis, either by using thermal treatment or a soft chemistry treatment in ethylene glycol.[7–8] Nanoparticles with at least two metallic elements were recently described in the literature and seem interesting enough.[9–10] The choice of metallic oxalato complexes anions to be trapped in the interlayer domain resulted in previous studies which permitted intercalation of two pure metallic oxalato complexes,[11–12] but also mixed LDH phases with impurities.[11] The particular choice of $[GaOx_3]^{3-}$, $[MnOx_3]^{3-}$, $[CuOx_2]^{2-}$, or $[CoOx_2]^{2-}$ anions depends on really interesting possibilities of the metal or even of the oxalato complex in catalysis.[13–26] The compound corresponding to $[CuOx_2]^{2-}$ intercalated between $[Zn_2Al]$ LDH layers will be abbreviated hereafter as $[Zn_2AlCu]$. In a same way we note for $[Zn_2Al]$ layers $[Zn_2AlCo]$, $[Zn_2AlGa]$, and $[Zn_2AlMn]$ and for $[Mg_2Al]$ layers $[Mg_2AlCu]$, $[Mg_2AlCo]$, $[Mg_2AlGa]$, and $[Mg_2AlMn]$, the obtained compounds with metallic complexes $[CoOx_2]^{2-}$, $[GaOx_3]^{3-}$ and $[MnOx_3]^{3-}$ respectively. This variety of metals could bring a large range of possibilities to create single or mixed oxides for practical applications.

2. Experimental Section

2.1. Sample Preparation. $[Zn_2AlCl]_{LDH}$ and $[Mg_2AlCl]_{LDH}$ with ideal formula $[Zn_2Al(OH)_6]Cl\cdot2H_2O$ and $[Mg_2Al(OH)_6]Cl\cdot2H_2O$, respectively, were used as precursors for the studies in intercalation of oxalate anions between LDHs layers.

2.1.1. Synthesis of Precursors. These precursors were prepared by a coprecipitation method to control pH.[27] Mixed solutions of $ZnCl_2$ (Prolabo)–$AlCl_3$ (Sigma 99%) and $MgCl_2$ (Sigma 98%)–$AlCl_3$ (Sigma 99%) with the required M^{II}/M^{III} ratio, having total cations concentrations equal to 1 M, have been used at constant pH 8.5 and 9.5, respectively, for $[Zn_2AlCl]$ and $[Mg_2AlCl]$ precursors. These preparations were performed under nitrogen atmosphere to prevent contamination by carbonate from atmospheric CO_2 at room temperature except for $[Mg_2AlCl]$ (which was prepared at 65 °C). For a higher positive charge of the layer, the value of the molar ratio M^{II}/M^{III} was fixed to 2; this permitted an interesting ratio between layer metals and intercalated metals corresponding to the best activities in basic and redox catalysis.[28–35]

2.1.2. Anionic Exchange. First, we tried unsuccessfully to realize a classical anionic exchange in aqueous solution. Even with important excess of anions in methanol, acetone, or ethylene glycol, we had no more results. So we developed a new way of synthesis using anionic exchange under hydrothermal conditions. Different parameters, such as heating duration, temperature, excess of anion to intercalate, and solution volume in autoclave were tested. In some cases classical anionic exchange was carried out at room temperature, under nitrogen atmosphere, during a well-defined time before the hydrothermal treatment.

Optimal parameters were determined for each compound (Table 1). As an example, the intercalation of $[MnOx_3]^{3-}$ anion in $[Mg_2Al]$ precursor is described below.

In a first step, a well-defined mixture of LDH precursor and $K_3Mn(C_2O_4)_3$ with 1.4 molar ratio excess was crushed in an agate mortar during five minutes and placed in an autoclave (22 cm³) with distilled and decarbonated water. The autoclave was then heated at 120 °C during 48 h developing autogenous pressure of about 2.4 kbar.

After autoclave quenching in water, powdered products were recovered by centrifugation. Three washing cycles with car-

(34) Jyothi, T. M.; Raja, T.; Talawar, M. B.; Rao, B. S. *Appl. Catal., A* **2001**, *211*, 41.

(35) Climent, M. J.; Corma, A.; Guil-Lopez, R.; Iborra S.; Primo, J. *Catal. Lett.* **1999**, *59*, 33.

Table 1. Synthesis Parameters for Exchanges LDH Samples

exchanged anion $[MOx_x]^{x-}$	molar excess of $[MOx_x]^{x-}$	θ °C of steamroom for hydrothermal treatment	duration of hydrothermal treatment	preliminary treatment[a]
A. [MgAl] Layer				
$[MnOx_3]^{3-}$	1.4	120	48 h	no
$[GaOx_3]^{3-}$	2.1	150	5 h 30 min	no
$[CoOx_2]^{2-}$	0.86	155	65 h	no
$[CuOx_2]^{2-}$	0.91	155	65 h	no
B. [ZnAl] Layer				
$[MnOx_3]^{3-}$	1.25–3.3	120	48 h	no
$[GaOx_3]^{3-}$	1.18	120	2 h 20 min	yes during 2 h
$[CoOx_2]^{2-}$	0.91	155	65 h	no
$[CuOx_2]^{2-}$	0.84	155	65 h	no

[a] Classical anionic exchange under nitrogen atmosphere.

bonate-free water were required, then the powders were dried in air at 50 °C during 12 h.

2.2. Characterization Techniques and Procedure. Powder X-ray diffraction patterns were performed on a Siemens D 501 X-ray diffractometer using Cu Kα radiation and fitted with a graphite scattered beam monochromator. The samples as unoriented powder were scanned from 2 to 76° (2θ) in steps of 0.08° with a count time of 4 s at each point. Fourier transform infrared spectra were obtained with a Perkin-Elmer 16PC spectrophotometer at a resolution of 2 cm^{-1} and averaging 10 scans in the 400–4000 cm^{-1} region on pressed KBr pellets. Thermogravimetry coupled with mass spectrometry were respectively recorded on a Setaram TG DTA 92 thermogravimetric analyzer at a typical rate of 5 °C min^{-1} under air/argon atmosphere and on Quadstar 422 Balzers. The nitrogen adsorption isotherms of the samples at liquid nitrogen temperature were recorded on a Coulter SA 100. Prior to a pretreatment, which consisted of a degassing period of 500 min at the temperature corresponding to the end of dehydration for each compound. This was done to remove the adsorbed and interlayer water, and to leave only anions in the interlayer space. The pore distribution in all samples was calculated using the BJH model on the desorption branch. Elementary analyses were performed at the Vernaison Analysis Center of CNRS. Particle size distributions were performed on a Malvern mastersizer 2000 using the accessory for powder. Zn K-edge, Cu K-edge, Co K-edge, Mn K-edge, and Ga K-edge XAFS (X-ray absorption fine structure) studies were performed at LURE (Orsay, France) using X-ray synchrotron radiation emitted by the DCI storage ring (1.85 GeV positrons, average intensity of 250 mA) at the D44 line. Data were collected at room temperature in transmission mode at the Zn K-edge (9.658 keV), Cu K-edge (8.978 keV), Co K-edge 7.708 keV), Mn K-edge (6.539 keV), and Ga K-edge (10.367 keV). The quantity of powered samples was chosen to obtain edge jumps of about $\Delta\mu x$ near 1. A double-crystal Si (111) monochromator scanned the energy in 2-eV (XAFS) or 0.5-eV (XANES) steps from 100 to 900 eV (XAFS) or 80 eV (XANES) above the absorption edges. Three spectra were recorded for each sample. An accumulator time of two seconds was used per point.

The analysis of the EXAFS data was performed following standard procedures for extraction of the signal and normalization to the edge adsorption. All the EXAFS spectra were treated by using the classical plane wave single scattering approximation. Fourier transforms of the EXAFS spectra were made after multiplication of the signal by a k^3 factor over a 2.8–14 Å^{-1} Kaiser apodization window with τ = 2.5 to determine electronic parameters, such as the scale factor (the intrinsic loss factor, S_o^2) and the Γ factor related to the mean free path λ of the photoelectron ($\lambda = k/\Gamma$). The contribution of oxygen atoms in $[Zn_2AlCl]$ then of carbon and metal atoms neighbors were extracted by a Fourier transform of $k^3 \chi(k)$ versus R (Å) curve back to the k space. The resultant $\chi(k)$ signal was fitted using the following formula:

$$\chi(k) = S_o^2 \sum A_i(k) \sin[2kr_i + \Phi_i(k)]$$

Table 2. Chemical Compositon of Exchanged LDHs and Proposed Formula

sample	ratio M^{II}/M^{III}	chemical analysis % and proposed formula				
[Mg$_2$AlCl]	2.06					
[Zn$_2$AlCl]	1.98					
[Mg$_2$AlCo]	1.94	C 9.65	H 2.66	Mg 17.50	Co 11.81	Al 10.83
		Mg$_{0.66}$Al$_{0.34}$(OH)$_2$[(C$_2$O$_4$)$_2$Co]$_{0.17}$·H$_2$O$_{0.12}$				
[Mg$_2$AlCu]	1.94	C 7. 84	H 2.48	Mg 15.78	Cu 10.37	Al 8.97
		Mg$_{0.66}$Al$_{0.34}$(OH)$_2$[(C$_2$O$_4$)$_2$Cu)]$_{0.17}$·H$_2$O$_{0.26}$				
[Mg$_2$AlGa]	1.94	C 6.87	H 2.49	Mg 13.08	Ga 6.71	Al 7.55
		Mg$_{0.66}$Al$_{0.34}$(OH)$_2$ [(C$_2$O$_4$)$_3$Ga]$_{0.12}$·H$_2$O$_{0.53}$				
[Mg$_2$AlMn]	1.94	C 8.16	H 2.58	Mg 16.12	Mn 6.22	Al 9.2
		Mg$_{0.66}$Al$_{0.34}$(OH)$_2$ [(C$_2$O$_4$)$_3$Mn]$_{0.11}$·H$_2$O$_{0.33}$				
[Zn$_2$AlCo]	1.89	C 6.47	H 1.81	Zn 32.54	Co 7.95	Al 7.14
		Zn$_{0.66}$Al$_{0.35}$(OH)$_2$[(C$_2$O$_4$)$_2$Co]$_{0.18}$·H$_2$O$_{0.19}$				
[Zn$_2$AlCu]	1.86	C 6.05	H 1.62	Zn 32.28	Cu 8.54	Al 7.29
		Zn$_{0.65}$Al$_{0.35}$(OH)$_2$[(C$_2$O$_4$)$_2$Cu)]$_{0.18}$·H$_2$O$_{0.06}$				
[Zn$_2$AlGa]	1.83	C 6.18	H 2.34	Zn 31.97	Ga 5.92	Al 7.19
		Zn$_{0.64}$Al$_{0.35}$(OH)$_2$ [(C$_2$O$_4$)$_3$Ga]$_{0.11}$·H$_2$O$_{0.54}$				
[Zn$_2$AlMn]	1.94	C 6.85	H 2.00	Zn 35.42	Mn 5.26	Al 7.48
		Zn$_{0.66}$Al$_{0.34}$(OH)$_2$ [(C$_2$O$_4$)$_3$Mn]$_{0.12}$·H$_2$O$_{0.23}$				

with the amplitude

$$A_i(k) = (N_i/kr_i^2)F(k)\exp(-2k^2\sigma_i^2)$$

where r_i is the interatomic distance, taken as the crystallographic data for the reference, Φ_i is the total phase shift of the ith shell, N_i is the effective coordination number, σ_i is the Debye–Waller factor and $F_i(k)$ is the backscattering amplitude. [Zn$_2$AlCl], K$_2$Cu(C$_2$O$_4$)$_2$, K$_2$Co(C$_2$O$_4$)$_2$, K$_3$Ga(C$_2$O$_4$)$_3$, and K$_3$Mn-(CN)$_6$ were taken as the reference materials. The theoretical functions from Mc Kale's tables were taken as the phase and amplitude.[36] The EXAFS signal treatments and refinements were performed with the program package developed by A. Michalowicz.[37] The residual ρ factor is defined as $\rho = [\Sigma(k^3\chi \exp(k) - k^3 \chi\text{theo}(k))^2]^{1/2}$. The commonly accepted fitting accuracy is about 0.02 Å for the distance and 10–20% for the number of neighbors.

3. Results and Discussion

3.1. Characterization of Exchanged Layered Double Hydroxides. *3.1.1. Chemical and XRD Analyses.* Chemical analysis and XRD study confirmed the reality of a full exchange of chloride anions by anionic oxalato complexes. Chemical compositions of obtained compounds are reported in Table 2 (nonstoechiometric formulas were suggested). They revealed that M^{II}/M^{III} molar ratios were close to LDH's chloride precursors values which excluded a partial dissolution of the divalent ion of the layers due to hydrothermal synthesis. Indeed the existence of defective sheets has already been noted for tetracyanoquinodimethane[38] and [RuCl$_5$H$_2$O][39] in [Zn$_3$Al] LDHs and reported for the synthesis of pillared clays with Keggin ions.[40] Chemical analysis revealed no carbonate contamination.

X-ray powder diffraction patterns of exchanged products are presented in Figure 1. All compounds crystallized with no remaining crystallized LDH chloride precursors. The best results obtained for the indexation correspond to a 3R stacking sequence ($R\bar{3}m$ space group
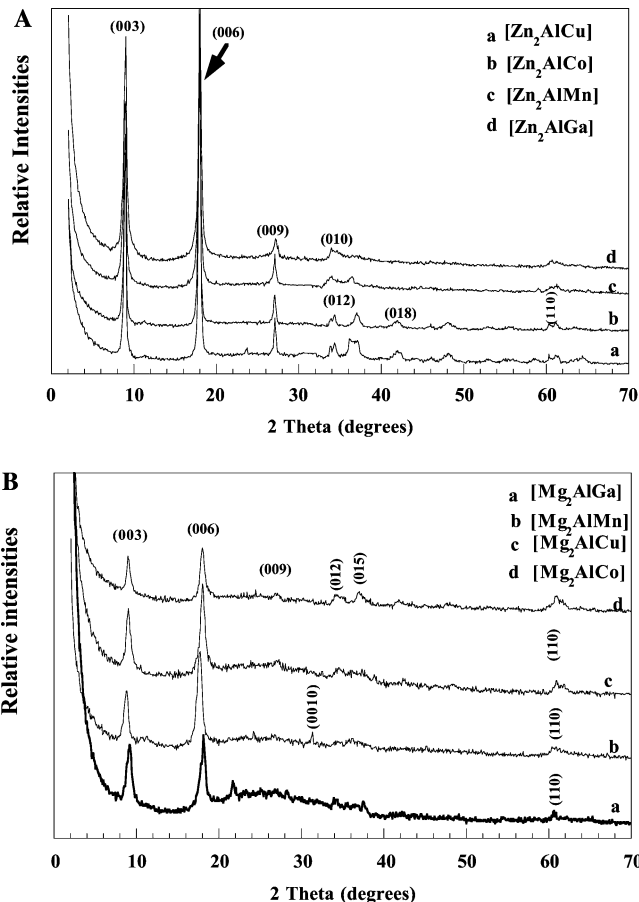
(36) MacKale, A. G.; Veal, B. W.; Paulikas, A. P.; Chan, S. K.; Knapp, J. *J. Am. Chem. Soc.* **1988**, *110*, 3763.
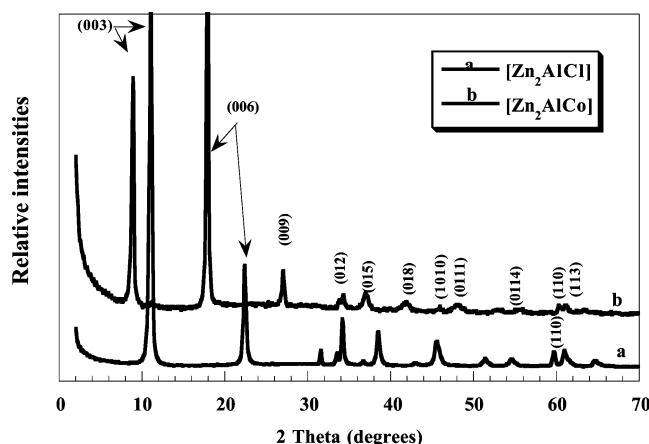(37) Mickalowicz, A. Programs available on the web site of lure. http:// www.lure.fr.
(38) Bonnet, S.; Forano, C.; Besse, J. P. *Mater. Res. Bull.* **1998**, *33*, 783.
(39) Inacio, J.; Taviot-Guého, C.; Morlat-Thérias, S.; de Roy, M. E.; Besse, J. P. *J. Mater. Chem.* **2001**, *11*, 640.
(40) Wang, J.; Tian, Y.; Wang, R. C.; Clearfield, A. *Chem. Mater.* **1992**, *4*, 1276.

Figure 1. Diffraction patterns of [Zn$_2$AlCu],; [Zn$_2$AlCo], [Zn$_2$AlMn], and [Zn$_2$AlGa] (A); and [Mg$_2$AlCu], [Mg$_2$AlCo], [Mg$_2$AlMn], and [Mg$_2$AlGa] (B).

with hexagonal axes (Table 3 and Figure 2)). For LDH, the c-parameter corresponds to three times the interlamellar distance $d_{(003)}$ and the a-parameter, which represents the average intermetallic distance, is calculated from the position of the $d_{(110)}$ ray. Cell parameters in precursors and in exchanged products are compared in Table 4. As expected, the exchange of anionic species between layers induced an increase of c-parameter. In contrast, we noted a decreasing a-parameter value in LDH intercalated by oxalato complexes comparatively to that of LDH chloride precursors. The nature of the intercalated complex has no major influence upon

Table 3. X-rays Peaks Indexation (Space Group $R\bar{3}m$)

(hkl)	[Zn$_2$AlCu] 2θ (°)	[Zn$_2$AlCo] 2θ (°)	[Zn$_2$AlMn] 2θ (°)	[Zn$_2$AlGa] 2θ (°)	[Mg$_2$AlGa] 2θ (°)	[Mg$_2$AlMn] 2θ (°)	[Mg$_2$AlCu] 2θ (°)	[Mg$_2$AlCo] 2θ (°)
(003)	9.06	9.04	9.04	9.2	9.28	8.92	9.12	9.04
(006)	18.06	18.08	18.08	18.16	18.23	17.78	18.09	18.08
(009)	27.19	27.12	27.2	27.28	28.19		27.17	27.12
(101)	33.91		33.85	34.00	33.96			
(012)	34.43	34.4	36.61			34.39	34.68	34.48
(0012)	36.45				37.55			
(015)	37.11	37.12				36.10	37.47	37.12
(018)	42.07	42.00					42.44	41.84
(1010)	46.10	46.16						
(0111)	48.21	48.24						
(0114)	55.48	55.44						
(110)	60.48	60.48	60.59	60.52	60.41	60.47	60.62	60.80
(113)	60.88	61.15	61.32	61.24	60.73	61.37	61.41	61.55
(116)		63.62						
(0117)	64.15							

Figure 2. Compared and indexed diffraction patterns of [Zn$_2$-AlCo] and [Zn$_2$AlCl] compounds.

Table 4. Cell Parameters and Basal Spacing (d) (Hexagonal Symmetry, Space Group $R\bar{3}m$)

sample	a (nm)	c (nm)	d (nm)
[Zn$_2$AlCl]	0.3089(1)	2.3715(7)	0.7905
[Zn$_2$AlCu]	0.3066(1)	2.9377(8)	0.9792
[Zn$_2$AlCo]	0.3059(8)	2.9454(9)	0.9818
[Zn$_2$AlMn]	0.3061(8)	2.9466(5)	0.9822
[Zn$_2$AlGa]	0.3062(9)	2.9404(6)	0.9801
[Mg$_2$AlCl]	0.3073(9)	2.3860(5)	0.7953
[Mg$_2$AlCu]	0.3052(3)	2.9515(4)	0.9838
[Mg$_2$AlCo]	0.3050(6)	2.9521(1)	0.9841
[Mg$_2$AlMn]	0.3062(0)	2.8790(2)	0.9596
[Mg$_2$AlGa]	0.3066(3)	2.8843(6)	0.9614

a-parameter ($\sim$0.306 nm) in compounds obtained from [Zn$_2$Al] precursor while a small influence of the oxidation number of the metal in oxalato complex appears in [Mg$_2$Al] compounds. However, the basal spacing values are rather similar for all the exchanged LDHs except for [Mg$_2$AlMn] and [Mg$_2$AlGa] for which it is slightly lower. This phenomenon will be discussed below.

For all the compounds, an inversion of intensity between the two first peaks (00l) in the exchanged products is observed, compared to that of the chloride LDHs precursors (Figure 2). This phenomenon appeared in previous works for LDHs containing heavy interlayer molecular species such as chromate or vanadate anions between [MgAl] layers,[27] [AlOx$_3$]$^{3-}$ anions between [Zn$_3$-Al] layers,[11] or hybrid hexa-chlorohydroxo-platinum anions between [Zn$_2$Al], [Mg$_2$Al], and [Cu$_2$Al] layers.[41]

A common feature on all the X-ray patterns is that the second (00l) diffraction line becomes stronger than the first one. This has been attributed to the electron density increase in the interlayers midpoint due to the heavy metal's presence. In this case, the XRD patterns show an important intensity ratio between (006) and (003) diffraction lines, which could be linked to the high electronic density of the intercalated metal.

In the precursor, the position commonly admitted for Cl$^-$ anion is the 18 g site of $R\bar{3}m$ space group.[26] For example, after exchanging Cl$^-$ anion by [CoOx$_2$]$^{2-}$, the ratio between the atomic scattering factors of cobalt atom and chloride anion is about 2.2 for the (006) diffraction lines according to the value $z = {}^{1}/_{2}$.

This would explain the observed inversion in the relative intensities of (003) and (006) diffraction lines between the precursor containing chloride anions and the exchanged phase containing metal complexes within the layers.

This phenomenon clearly points out the presence of a heavy atom between the layers.

3.1.2. FT-IR Characterization. Previous works [42–45] give the characteristic bands of metallic anionic oxalato complexes which are listed in Table 5A. Experimental bands of LDH intercalated products are reported in Table 5B. LDH intercalated products correspond to compounds free of carbonate contamination: the $v_3(CO_3^{2-})$ band around 1375 cm^{-1} does not appear.

The main absorption band centered in the 3500–3400 cm^{-1} region corresponds to the vibration v (OH) of hydroxyl groups from the brucite-like layers as well as from the interlamellar water molecules. The other intense bands at 1620 cm^{-1}, which are normally observed for LDHs compounds, concern the vibration resulting from the water molecule δ (H$_2$O); in our case, we observe a superposition of the previous bands with the very intense bands of metallic oxalato complexes v_a-(C=O). Between 1650 and 1290 cm^{-1}, the three characteristic bands of intercalated metallic oxalato com-

(41) Beaudot, P.; de Roy, M. E.; Besse, J. P. *J. Solid State Chem.* **2001**, *161*, 332.

(42) Nakamoto, K. *Infrared and Raman Spectra of Inorganic and Coordination Compounds*, 4th ed.; Wiley: New York, 1986; part B, p 74.

(43) Fujita, J.; Martell, A. E.; Nakamoto, K. *J. Chem. Phys.* **1962**, *36*, 324.

(44) Edwards, H. G. M.; Hardman, P. H. *J. Mol. Struct.* **1992**, *273*, 73.

(45) Edwards, H. G. M.; Farwell, D. W.; Rose, S. J.; Smith, D. N. *J. Mol. Struct.* **1991**, *249*, 233.

Table 5. Infrared Bands Data

A: For Metallic Oxalato Complexes

band	$K_2[Cu-(C_2O_4)_2]\cdot2H_2O$ (cm^{-1})	$K_2[Co(C_2O_4)_2]\cdot2H_2O$ (cm^{-1})	$K_3[Ga(C_2O_4)_3]\cdot3H_2O$ (cm^{-1})	$K_3[Mn(C_2O_4)_3]\cdot3H_2O$ (cm^{-1})
v(OH)	3472	3380	3532	3365
v_a(C=O) v_7	1672	1622	1722	1643
v_a(C=O) v_1	1645	1614	1702−1653	
v_5(CO) + v(CC) v_2	1411	1364	1405	1454
v_S(CO) + δ (O−C=O) v_8	1277	1316	1295−1265	1304
v_S(CO) + δ (O−C=O) v_3	886	827	907	887
δ (O−C=O) + v(MO) v_9	795	790	820−803	780
v(MO) + v(CC) v_4	539	499	588	519
δ (O−C=O) v_{10}	481	429		519
v(MO) v_{11}			499	

B: For Intercalated Compounds

LDH	v(OH) (cm^{-1})	δ (H$_2$O) (cm^{-1})	v_a (C=O) (cm^{-1})	v_5(CO) + v(CC) (cm^{-1})	v_S(CO) + δ (O−C=O) v_8 (cm^{-1})	v_{M-O} (cm^{-1})	δ_{O-M-O} (cm^{-1})
[Zn$_2$AlCo]	3522	1653	1623	1354	1314	598	430
[Mg$_2$AlCo]	3522	1643	1623	1354	1314	590	400
[Zn$_2$AlCu]	3482	1623	1623	1434	1324	608	439
[Mg$_2$AlCu]	3462	1623	1623	1434	1324	600	419
[Zn$_2$AlGa]	3482	1633	1633	1384	1324	658	459
[Mg$_2$AlGa]	3482	1613	1613	1384	1324	618	419
[Zn$_2$AlMn]	3472	1623	1623	1424	1324	618	419
[Mg$_2$AlMn]	3472	1623	1623	1424	1324	580	420

Table 6. Results of EXAFS Study for Zn Atom Local Environment in Layers[a]

compound	N_1=N_2	R_1 nm	σ_1 10^{-4} nm^2	F	R_2 nm	$\sigma_2$10^{-4} nm^2	F
[Zn$_2$AlCl]	6.02	0.205	3.2	3.18 10^{-2}	0.308(3)	8	5.78 10^{-2}
[Zn$_2$AlCu]	6.02	0.206	3.2	3.55 10^{-2}	0.310(1)	8	5.94 10^{-2}
[Zn$_2$AlCo]	6.02	0.206	3.2	2.94 10^{-2}	0.309(3)	8	5.06 10^{-2}
[Zn$_2$AlGa]	6.00	0.208	3.2	1.64 10^{-2}	0.309(4)	8	6.01 10^{-2}
[Zn$_2$AlMn]	6.00	0.208	3.2	2.68 10^{-2}	0.308(1)	8	6.06 10^{-2}

[a] σ_i, Debye−Waller factor (fixed); N_i, effective coordination number; R_i, interatomic distance between studied atom and its neighbor (Å); F, disagreement factor.

plexes appear, respectively, due to v_a(C=O), v_5(CO) + v(CC), and v_S(CO) + δ (O−C=O) vibrations. Other less intense characteristic bands of metallic oxalato complexes appear between 900 and 400 cm^{-1}.

So, it is clear that metallic oxalato complexes preserved their structural characteristics, without modification due to hydrothermal conditions.

The bands in the range of 700−500 cm^{-1} characteristic of LDHs structure correspond to the vibration v_{M-O} (M = layer's metal); the deformation vibration bands δ_{O-M-O} are located around 425 cm^{-1}.

The IR spectra between 400 and 4000 cm^{-1} are typical of LDH and confirmed the effective intercalation of metallic oxalato complexes between LDH layers.

3.1.3. X-ray Absorption Spectroscopy. A study at the ZnK-edge carried out on [Zn$_2$AlCl] and all the Zn-containing compounds shows that all the pseudo radial distribution functions are superimposed. So it seems that, during exchange, no modifications occurred concerning the local order around the layers Zn atoms; that is six oxygen atoms about 0.2 nm and six metallic atoms about 0.31 nm. Simulation results are presented in Table 6. In the same way and according to chemical analysis results, preservation of [Mg$_2$Al] layers could be a reasonable hypothesis.

To study interlamellar metals environment in complexes, X-ray absorption spectra were also recorded at the K-edge of Cu, Co, Ga, and Mn atoms.

[Cu(C$_2$O$_4$)$_2$]$^{2-}$ Anion. Projection of the well-known [Cu(C$_2$O$_4$)$_2$]$^{2-}$ anion's structure[44,45] is presented in Scheme 1. Simulation carried out on reference compound: K$_2$-[Cu(C$_2$O$_4$)$_2$]·2H$_2$O permitted fixing of parameters (ex-
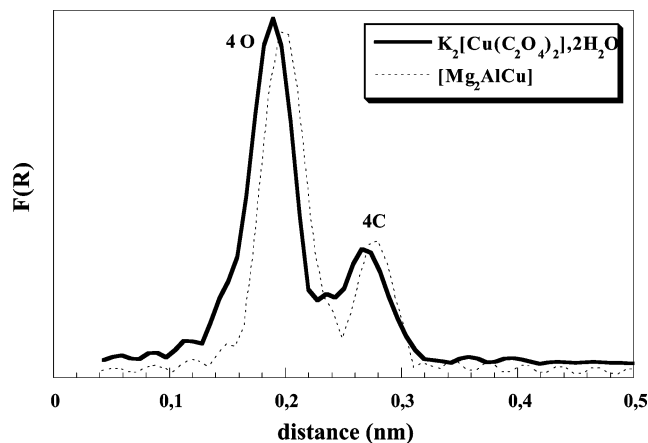
Figure 3. Comparison of Fourier transform curves of [Mg$_2$-AlCu] and K$_2$[Cu(C$_2$O$_4$)$_2$]·2H$_2$O.

cepting distance and number of neighbors) used for exchanged LDHs study. Results are presented in Table 7.

It is noteworthy that the [Cu(C$_2$O$_4$)$_2$]$^{2-}$ structure is preserved but with increasing Cu−O(1) and Cu−C distances for [Mg$_2$AlCu] compound, indicating a significant interaction between layers and intercalated complexes (Figure 3).

We did not obtain results concerning the third coordination shell of copper in the reference compound as it was previously reported in the literature.[46] But, these results concerning intercalated products are presented in Table 7 and Figure 4.

Measured distances Cu−O(2) are similar enough to the literature value: 0.390 nm in K$_2$[CuOx$_2$]·2H$_2$O.

Table 7. Results of EXAFS Study for Cu Atom Local Environment

compound	N_1	R_1 nm (Cu−O(1))	N_2	R_2 nm (Cu−C)	N_3	R_3 nm (Cu−O(2))	$\sigma_1=\sigma_2=\sigma_3$ 10^{-4} nm²	F_1 10^{-2}	F_2 10^{-2}	F_3 10^{-2}
$K_2[Cu(C_2O_4)_2]\cdot2H_2O$	4.01	0.193	4.01	0.270			2.4	1.99	3.71	
$[Zn_2AlCu]$	4.00	0.196	4.00	0.274	4.00	0.395	2.4	0.853	3.03	5.62
$[Mg_2AlCu]$	3.99	0.197	4.00	0.276	4.00	0.380	2.4	3.33	3.55	5.84

Table 8. Results of EXAFS Study for Co Atom Local Environment

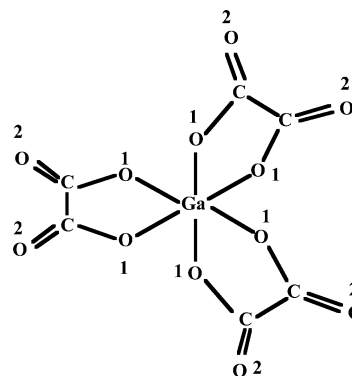| compound	N_1	R_1 nm (Co−O(1))	N_2	R_2 nm (Co−C)	N_3	R_3 nm (Cu−O(2))	$\sigma_1=\sigma_2=\sigma_3$ 10^{-4} nm²	F_1 10^{-2}	F_2 10^{-2}	F_3 10^{-2}
$K_2[Co(C_2O_4)_2]\cdot2H_2O$	3.99	0.209	4.01	0.285	4.00	0.391	8.4	1.66	5.21	5.71
$[Zn_2AlCo]$	3.99	0.212	4.00	0.288	4.00	0.394	8.4	1.29	5.03	5.29
$[Mg_2AlCo]$	4.00	0.211	4.00	0.287	4.00	0.381	8.4	1.46	4.35	3.89
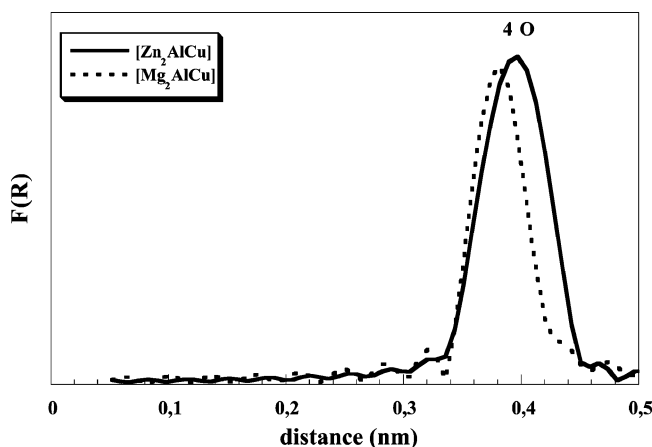
Figure 4. Comparison of Fourier transform curves of [Mg₂AlCu] and [Zn₂AlCu] on the third coordination shell.
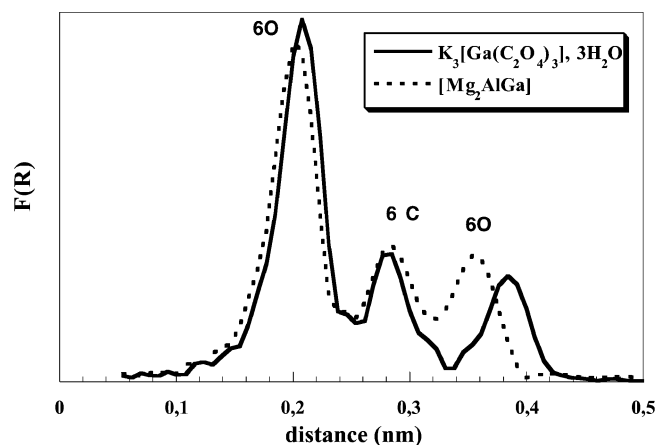
Figure 5. Comparison of Fourier transform curves for K₃[Ga(C₂O₄)₃]·3H₂O and [Mg₂AlGa].

Scheme 1. [Cu(C₂O₄)₂]²⁻ Projection Plane

Scheme 2. [Ga(C₂O₄)₂]³⁻ Projection Plane
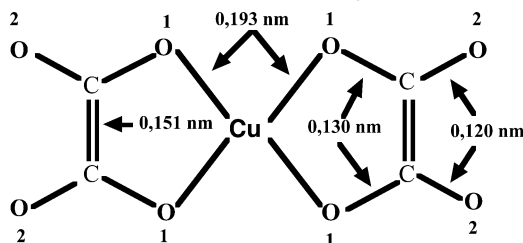
However, the small value obtained for the [Mg₂AlCu] compound is in favor of stronger interactions between metallic complexes and [Mg₂Al] layers than with [Zn₂Al] layers, as will be discussed below.

[Co(C₂O₄)₂]²⁻ Anion. Results obtained for the first, second, and third shells of cobalt coordination are listed in Table 8. It appeared that the cobalt environment was preserved with variations of Co−O and Co−C distances that were small compared to those of the reference compound K₂[CoOx₂]·2H₂O.

[Ga(C₂O₄)₃]³⁻ Anion. Structures of trivalent metallic oxalato complexes are well-known (Scheme 2), and distances values of first neighbors are in the range of 0.195−0.206 nm.[47]

The Ga atom environment in [Mg₂AlGa] is compared with that of the reference compound K₃[GaOx₃]·3H₂O in Figure 5. This structure was preserved after intercalation of [GaOx₃]³⁻ between both [Zn₂Al] and [Mg₂-Al] layers (Table 9). However, it is noteworthy that the third coordination shell was disturbed, showing two oxygen atoms at 0.322 nm and four oxygen atoms at 0.346 nm, inducing probable modifications of angles in the complex. In this case the interactions of both [Zn₂-

Al] layers and [Mg₂Al] layers on the [GaOx₃]³⁻ complex seem to be similar.

[Mn(C₂O₄)₃]³⁻ Anion. Because of the high instability of K₃[MnOx₃]·3H₂O,[48] no XAFS measurements were carried out on this compound, and we have considered that the [MnOx₃]³⁻ anion was structured as the [GaOx₃]³⁻ anion.

Otherwise a XANES study was carried out on MnOx₃³⁻ exchanged HDLs with K₃[Mn(CN)₆] as reference to confirm oxidation state III for the manganese atom in these compounds (Figure 6). The energy step was observed at 6550 eV for each compound, showing that the manganese oxidation state was preserved during intercalation. Results of the XAFS study are reported in Table 10, showing similar first and second coordination shells around the Mn atom comparatively to the Ga atom in intercalated oxalato complexes. However, the third coordination shell is quite different from that of the gallium oxalate ion (Table 10 B): it is composed
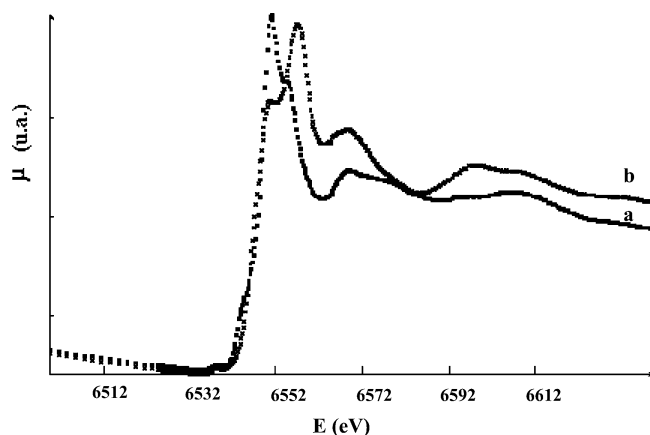
Figure 6. Comparison of Xanes curves of $K_3[Mn(CN)_6]$ (a) and $[Zn_2AlMn]$ (b).

Table 9. Results of EXAFS Study for Ga Atom Local Environment

A: For the Two First Coordination Shells

compound	N_1	R_1 nm (Ga−O(1))	N_2	R_2 nm (Ga−C)	$\sigma_1 = \sigma_2$ 10^{-4} nm^2	F_1	F_2 10^{-2}
$K_3[Ga(C_2O_4)_3]\cdot$ 3H$_2$O	6	0.198	6	0.274	4.83	7.2 10^{-3}	4.72
$[Zn_2AlGa]$	6	0.197	6	0.274	4.83	1.47 10^{-2}	3.64
$[Mg_2AlGa]$	6	0.196	6	0.274	4.83	1.87 10^{-2}	4.82

B: For the Third Coordination Shell

compound	N_{3-1}	R_{3-1} nm (Ga−O(2))	N_{3-2}	R_{3-2} nm (Ga−O(2))	$\sigma_{3-1} = \sigma_{3-2}$ 10^{-4} nm^2	F
$K_3[Ga(C_2O_4)_3]\cdot$ 3H$_2$O	6	0.376	0		4.83	2.69 10^{-2}
$[Zn_2AlGa]$	2	0.322	4	0.347	4.83	3.48 10^{-2}
$[Mg_2AlGa]$	2	0.320	4	0.344	4.83	4.87 10^{-2}

Table 10. Results of EXAFS Study for Mn Atom Local Environment

A: For the Two First Coordination Shells

compound	N_1	R_1 nm (Mn−O(1))	σ_1 10^{-4} nm^2	F_1	N_2	R_2 nm (Mn−C)	σ_2 10^{-4} nm^2	F_2
$[Zn_2AlMn]$	6	0.199	2.00	4.48 10^{-2}	6	0.278	2.00	5.68 10^{-2}
$[Mg_2AlMn]$	6	0.198	2.00	5.07 10^{-2}	6	0.278	2.00	5.97 10^{-2}

B: For the Third Coordination Shell

compound	$N_{3-1} = N_{3-2}$	R_{3-1} nm (Mn−O(2))	R_{3-2} nm (Mn−O(2))	$\sigma_{3-1} = \sigma_{3-2}$ 10^{-4} nm^2	F_3
$[Zn_2AlMn]$	3	0.332	0.354	2.00	5.17 10^{-2}
$[Mg_2AlMn]$	3	0.330	0.351	2.00	5.05 10^{-2}

with 3 oxygen atoms at 0.331 nm and 3 oxygen atoms at 0.354 nm.

For the same LDH host net, according to the nature of the trivalent metal Mn or Ga, different surroundings are observed in the intercalated oxalato complexes. The distribution of the six oxygen atoms involved in the third coordination shell is clearly different, with the best tested hypothesis leading to « 3−3 » and « 2−4 » distributions for $[MnOx_3]^{3-}$ and $[GaOx_3]^{3-}$, respectively.

3.1.4. Layout of Intercalated Complexes between the Layers. We tried to model the layout of metallic oxalato complexes between the layers by using the results presented above, which can be summarized as follows:

(a) intercalated metallic complexes take place in the middle of the interlayer; (b) small modifications of angle values in (C_2O_4) groups exist according to possible interactions with layers; and (c) the structural environment of intercalated metal and basal spacing values are clearly defined from XAFS and XRD studies.

The intercalation model used to obtain the free interlamellar space (d_{free}) was based on the equation $d_{free} = d_{obs} - (T_{Layer} + 2L_H)$. T_{Layer} corresponds to the thickness of the layer consisting of $[MO_6]$ octahedra; previous studies have shown that this thickness is nearly the same whatever the choice of LDH layer elements (about 0.20 nm).[49−51] L_H corresponds to hydrogen bond length between the layers and the anionic species (about 0.27 nm).[52]

As observed in Table 4, the basal spacing values for LDHs intercalated by metallic oxalato complexes are very similar (∼0.98 nm), except for $[Mg_2AlGa]$ and $[Mg_2AlMn]$ (∼0.96 nm). This weak difference suggests that all the complexes have nearly the same orientation in the interlamellar space, which could depend on the position of (C_2O_4) groups.

Concerning the bivalent anionic metallic oxalato complexes, a rapid calculation showed that we could not accept the hypothesis of (C_2O_4) groups parallel with the layers, so having (C_2O_4) groups quasi-perpendicular to the layers was the only possibility.

As it appears in Scheme 1, the literature[47] indicates that the two (C_2O_4) groups present different angle values relative to the projection plane, for example 12° and 24° for $K_2 [Cu(C_2O_4)_2]\cdot 2H_2O$. These values seemed to depend on the cation's nature. It was also pointed out that $(O(1)-M^{II}-O(1))$ angle values in the same (C_2O_4) group and angle value between two (C_2O_4) groups could vary.

This phenomenon is clearly confirmed by some of our results. Indeed, IR spectroscopy pointed out a small shift for the characteristic bands for metallic oxalato complexes intercalated products compared to that for free complexes (Table 5). XAFS study showed that, for example, the Cu−O(1) bond length in intercalated products increased compared to that with $K_2[Cu(C_2O_4)_2]\cdot 2H_2O$ (Table 7). These results are in accordance with a smaller value of $(O(1)-M^{II}-O(1))$ angle for intercalated complexes. This was already reported by Wickoff[53] for the $[Zn((C_2O_4)_2]^{2-}$ anion, in which $(O(1)-Zn-O(1))$ angle value was 71°.

The ideal (C_2O_4) group's size calculated with this angle value is in accordance with a perpendicular arrangement of metallic oxalato complexes in the interlamellar area.

All theis information suggests that the (C_2O_4) group could be compressed, leading to an adaptability of the oxalate structure without destruction.

Remark: We did not use the third neighbor atoms O(2) for basal spacing evaluation because the literature reports that distance O(2)−O(2) is smaller than the

(46) Michalowicz, A. *Thèse de doctorat d'état de l'Université Paris Val de Marne.* France, 1990.

(47) Wyckoff, R. W. G. *Crystal Stuctures*, 2nd ed.; Interscience Publishers: New York, 1966; vol. 5, pp 418−419.

(48) Carteledge, G. H.; Ericks, W. P. *J. Am. Chem. Soc.* **1936**, *58*, 2061.

(49) El Malki, K.; Guenane, M.; Forano, C.; de Roy, A.; Besse, J. P. *Mater. Sci. Forum* **1992**, *91*, 171.

(50) Bonnet, S.; Forano, C.; de Roy, A.; Besse, J. P.; Maillard, P.; Momenteau, M. *Chem. Mater.* **1996**, *8*, 952.

(51) Ennadi, A.; Khaldi, M.; de Roy, A.; Besse, J. P. *Mol. Cryst. Liq. Cryst.* **1994**, *244*, 373.

(52) Meyn, M.; Beneke, K.; Lagaly, G. *Inorg. Chem.* **1993**, *32*, 1209.

(53) Wyckoff, R. W. G. *Crystal Stuctures*, 2nd ed.; Interscience Publishers: New York, 1966; vol. 5, p 42.

Scheme 3. (A) Proposition for the Layout of a [M^{II}Ox$_2$]$^{2-}$ Anion between LDHs Layers; (B) Proposition for the Layout of a [M^{III}Ox$_3$]$^{3-}$ Anion between LDHs Layers (3–3 Distribution); (C) Proposition for the Layout of a [M^{III}Ox$_3$]$^{3-}$ Anion between LDHs Layers (2–4 Distribution)
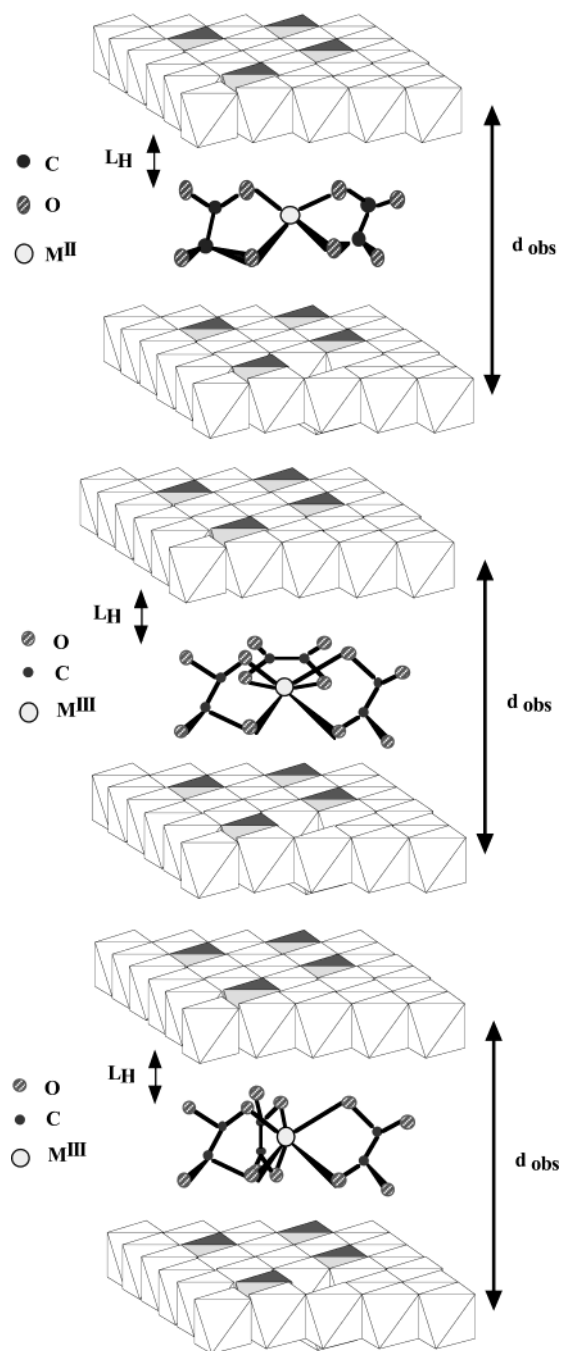
distance O(1)–O(1) of 0.010 nm, and because XAFS studies showed an oxygen atom's mobility with non-identifiable directions.

XAFS studies suggested also a more important effect of [Mg$_2$Al] layers than [Zn$_2$Al] layers on the third neighbors atoms O(2) positions (Tables 7–10). The effect of the layers' basicity is evident: indeed, [Mg$_2$Al] layers imposed smaller basal spacing (0.96 nm) than [Zn$_2$Al] layers (0.98 nm) (Table 4). It appeared that there were no consequences in the basal spacing for bivalent metallic oxalato complexes intercalates contrary to trivalent metallic oxalato complexes intercalates. Bivalent metal-
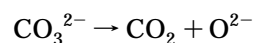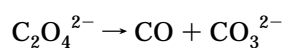
Table 11. TGA Study Results

LDH	temperature range (°C)	observed step	exp. loss of weight (%)	calc. loss of weight (%)
[Zn$_2$AlCu]	20–170	dehydration	3.6	3.7
	170–650	dehydroxylation + anion decomposition	32.6	32.8
[Mg$_2$AlCu]	20–140	dehydration	5.0	4.8
	140–750	dehydroxylation + anion decomposition	38.8	39.4
[Zn$_2$AlCo]	20–170	dehydration	2.9	2.7
	170–550	dehydroxylation + anion decomposition	33.8	34.0
[Mg$_2$AlCo]	20–130	dehydration	2.4	2.2
	130–700	dehydroxylation + anion decomposition	41.2	41.7
[Zn$_2$AlGa]	20–130	dehydration	7.5	7.4
	130–700	dehydroxylation + anion decomposition	33.3	33.0
[Mg$_2$AlGa]	20–210	dehydration	9.0	8.8
	210–720	dehydroxylation + anion decomposition	41.2	41.2
[Zn$_2$AlMn]	30–170	dehydration	3.5	3.3
	170–720	dehydroxylation + anion decomposition	34.2	34.2
[Mg$_2$AlMn]	30–150	dehydration	5.5	5.1
	150–750	dehydroxylation + anion decomposition	42.6	42.7

lic oxalato complexes could have better mobility in the interlamellar domain than trivalent metallic oxaloto complexes, which could permit balancing of the compression interactions. Layouts of these complexes in interlamellar domain are proposed in Scheme 3A, B, and C.

3.1.5. TG–MS Analysis. Thermal decomposition of hydrotalcite-like compounds is well described in the literature,[41,54–56] and particularly by Prevot et al. concerning oxalato complexes intercalated in LDH.[11] Generally, two steps of dehydration are observed: the dehydration of water molecules physisorbed at the external surface of the crystallites, and dehydration of intercalated water molecules more strongly attached to the network with hydrogen bonds. For the majority of intercalates studied in this paper, these two phenomena are not really separated and are observed in the temperature range of 30–200 °C depending on the host matrix (Table 11). At higher temperatures, the two steps corresponding to the dehydroxylation of the host matrix and the decomposition of oxalato complexes overlap each other.

The corresponding mass spectrometry for decomposition products was performed for [Zn$_2$AlMn] focused on some ions and molecules such as HCl and Cl$^-$ in order to detect possible remaining chloride precursor phases; H$_2$O, OH$^-$, and O^{2-} in order to know how water removes and decomposition of layers occurs; and C, CO, and CO$_2$ for oxalato complexes decomposition. These curves (Figure 7) indicate that dehydroxylation and complex decomposition take place around 320 °C, but the last phenomemon occurs on a larger temperature domain. Indeed, the CO$_2$ curveshows two clear decomposition steps at 320 and 480 °C, whereas TG analysis and the literature[16] mention only one step in the range 215–320 °C for decomposition of the metallic oxalato complex. Nevertheless the decomposition scheme of the (C$_2$O$_4$) group from a metallic oxalato complex is usually proposed as the following:
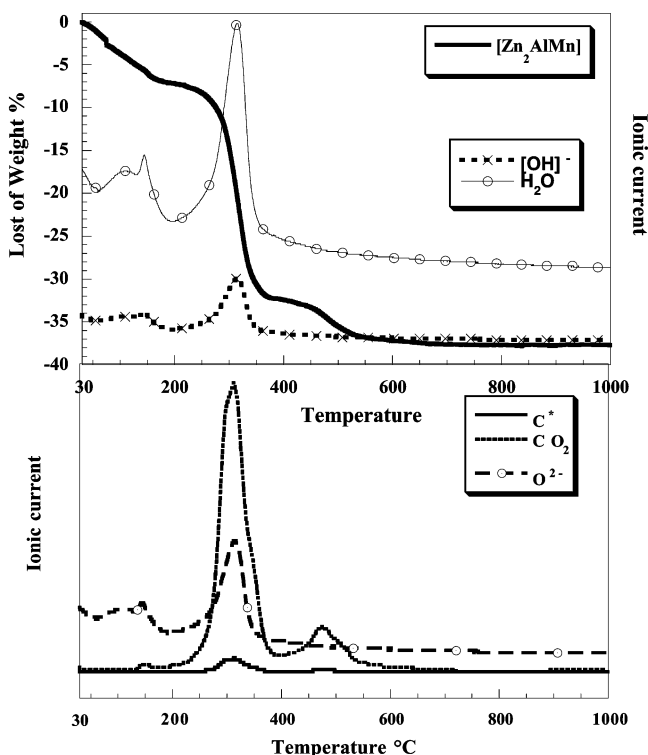
$$C_2O_4^{2-} \rightarrow CO + CO_3^{2-}$$

$$CO_3^{2-} \rightarrow CO_2 + O^{2-}$$

LDHs with Metallic Oxalato Complexes

Chem. Mater., Vol. 16, No. 5, 2004 943

Figure 7. Mass spectrometry and TGA curves for [Zn$_2$AlMn].

Table 12. Temperature of Appearance of Oxides Obtained after LDH Calcinations (°C)

	ZnO	MgO	Zn-Al$_2$O$_4$	Mg-Al$_2$O$_4$	CuO	CoO	Co$_2$O$_3$	Ga$_2$O$_3$	Mn$_2$O$_3$
[Zn$_2$AlCu]	200		900		800				
[Mg$_2$AlCu]		800.			1050				
[Zn$_2$AlCo]	200		900			700	700		
[Mg$_2$AlCo]		700				.	800		
[Zn$_2$AlGa]	500		900					800	
[Mg$_2$AlGa]		400						900	
[Zn$_2$AlMn]	400		800						900
[Mg$_2$AlMn]		400		700					900

showing that low-temperature calcinations led to amorphous phases. At temperatures higher than 300 °C, the layered structure collapsed and only small peaks were observed, which correspond to diffraction rays of MgO-like compounds or intercalated metal oxides depending on the layer composition. Calcination at 900 °C led to crystallization of well-defined phases for [Zn$_2$Al] compounds, while badly crystallized oxides were formed for [Mg$_2$Al] compounds (except [Mg$_2$AlMn]). This will be discussed below.

According to the results presented in Table 12, two conclusions can be pointed out as follows: (1) Intercalated metallic oxalato complexes have higher thermal stability than free complexes, as it was clearly shown for example by [Zn$_2$AlCu] and [Mg$_2$AlCu] calcinations. CuO appeared at about 800 °C instead of 350 °C for copper oxalate anion studied by Donia.[16] (2) [Mg$_2$Al] layers present a more important thermal stability than [Zn$_2$Al] layers as reported earlier for LDH phases containing simple inorganic anions such as chloride.

Otherwise, LDH phases intercalated by a trivalent metallic oxalato complex, particularly with gallium, have higher thermal stability than LDH phases intercalated with a bivalent metallic oxalato complex (for [Mg$_2$AlGa] the structure was preserved to about 350 °C, whereas it was destroyed at about 150 °C for copper and cobalt phases).

For [Mg$_2$AlMn], MgAl$_2$O$_4$ spinel phase appeared at temperatures as low as 700 °C instead of about 1200 °C as generally expected for [MgAl]$_{LDH}$. Two explanations could be pointed out: the effect of the nature of the intercalated metal or the formation of a Mn-doped spinel phase.

3.2.2. N2 Volumetric and Size Measurements. Synthetic LDH compounds are widely used as precursors for the preparation of mixed oxide catalysts;[57] so we carried out a systematic analysis of the nitrogen adsorption/desorption of LDHs intercalated with metallic oxalato complexes. The N$_2$ adsorption/desorption curves of compounds at several temperatures are typical of mesoporous materials (type IV in Brunauer, Deming, and Teller classification[58]); one example is shown in Figure 8. A similar behavior was described for LDH reference materials such as [Zn$_2$Al] and [Mg$_2$Al] containing chloride, carbonate,[58] or platinum complex anions[41] (25 m^2/g and 44 m^2/g, respectively, at 25 °C).

In most cases, the exchange of chloride anions by metallic oxalato complex had no significant effect on the

We observed a disproportion of peaks intensities at 320 and 480 °C in favor of the first, so we attributed the second peak to carbonate anion or (C$_2$O$_4$)$^{2-}$ trapped in the decomposed structure. On the basis of the study of [Zn$_3$AlCO$_3$] decomposition by Prévot[55] showing two mass spectrometry peaks in CO$_2$ curves, we supposed that CO$_3^{2-}$ anions were trapped in the oxide mixture during thermal treatment rather than (C$_2$O$_4$)$^{2-}$ groups. The really weak amount of observed CO could be due to the rather weak oxidant air/argon atmosphere (curves not reported).

XRD results did not reveal the presence of intermediary carbonated LDH phases, as was reported by Traversa[56] during the decomposition of [Mg$_3$Al] LDH phase intercalated by simple oxalate anion.

In accordance with XRD characterizations no chlorine was observed.

Using chemical analysis and TGA results, we calculated the weight loss corresponding to major steps of thermal decomposition, and the values are listed in Table 11 and compared with measured values.

3.2. Characterization of Layered Double Hydroxides upon Thermal Treatment. *3.2.1. XRD Characterization.* XRD patterns of exchanged compounds heated in air (24 h) at different temperatures in the range of 25−1050 °C were recorded. The total decomposition of LDHs leads to a mixture of divalent metal oxides, spinel phases, and, in some cases, oxides of trivalent metal.

The LDH structure was retained for some compounds, although the peaks were broader and less defined

(54) de Roy, A.; Vernay, A. M.; Besse, J. P.; Thomas, G. *Anulisis* **1988**, *16* (7), 409.

(55) Prévot, V.; Forano, C.; Besse, J. P. *J. Mater. Chem.* **1999**, *9*, 155.

(56) Traversa, E.; Nunziante, P.; Ghozzini, G. *Thermochim. Acta* **1992**, *199*, 25.

(57) Vaccari, A., Ed. *Synthesis and Applications of Anionic Clays*; Elsevier: Amsterdam, 1995.

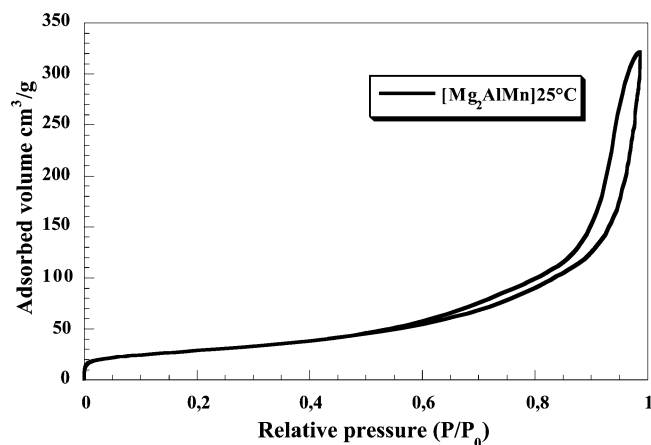(58) Brunnauer, S.; Deming, L. S.; Deming W. S.; Teller, E. *J. Am. Chem. Soc.* **1940**, *62*, 1723.

Figure 8. N_2 adsorption/desorption isotherms of noncalcined [Mg$_2$AlMn].

Table 13. Specific Surface Areas (BET, m²/g) Measured for Intercalates and Calcined Phases

	thermal treatment temperature (°C)		
	25	300	700
[Zn$_2$AlCu]	27.1	47.1	28.1
[Mg$_2$AlCu]	43.3	54.2	76.4
[Zn$_2$AlCo]	27.8	47.2	28.3
[Mg$_2$AlCo]	47.3	56.8	119.3
[Zn$_2$AlMn]	29.1	38.4	38.0
[Mg$_2$AlMn]	54.8	52.8	101.9
[Zn$_2$AlGa]	27.8	36.6	50.9
[Mg$_2$AlGa]	78.6	63.0	131.2

surface area, except for [Mg$_2$AlMn] and [Mg$_2$AlGa] compounds as shown from results presented in Table 13.

For compounds heated at 300 °C, different behaviors occur: we observed an increasing of surface area values for [Zn$_2$Al] compounds corresponding to the beginning of thermal decomposition. In the same way, we noted that, at 200 °C, oxides as ZnO started to crystallize. In contrast, for [Mg$_2$Al] phases calcined at 300 °C, the specific surface areas were not significantly modified for [Mg$_2$AlCu] and [Mg$_2$AlCo], while a decrease occurred for trivalent metallic oxalato complexes containing compounds. This points out that the LDH structure was partly preserved, while the interlamellar domain appeared disorganized according to dehydroxylation.

Increasing calcination temperature from 300 to 700 °C induced an increase in BET surface areas for all [Mg$_2$Al] compounds; the most important effect was obtained for [Mg$_2$AlMn] and [Mg$_2$AlGa]. Concerning [Zn$_2$Al] compounds, calcinations at 700 °C induced a decrease in BET surface areas for [Zn$_2$AlCu] and [Zn$_2$AlCo]. This phenomenon is directly connected to the oxides crystallization in this temperature range. For [Zn$_2$AlMn], no significant modifications appeared, while a small increase in surface areas occurred for [Zn$_2$AlGa].

On the basis of this study, it seems that optimal values for BET surface areas could be obtained for calcination temperatures around 600 °C.

For intercalated LDHs, at 25 °C, BJH studies concerning the pore sizes showed a mesoporous behavior (60−70%) with a large range of sizes for bivalent metallic oxalato complexes (Figure 9). However, for [Mg$_2$AlMn] and [Mg$_2$AlGa] we noted a more important proportion of micropores (30−40%). However, Groen[62] recently reported that the BJH method was not the most
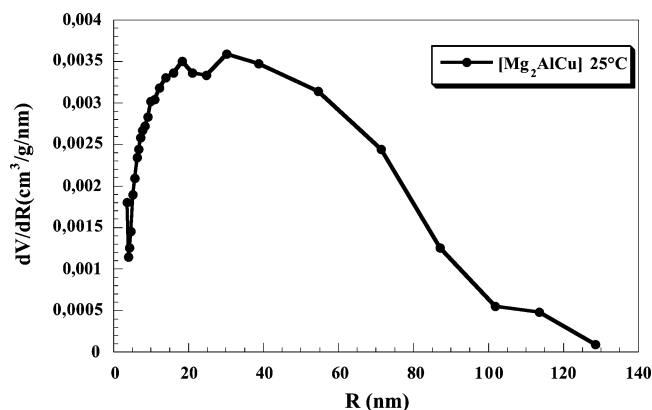

Figure 9. Pore size distribution for [Mg$_2$AlCu].

Table 14. Laser Diffraction Particles Sizing for Noncalcined Compounds

	aggregates size average (μm)	
LDH	first type	second type
[Zn$_2$AlCl]	3.2	
[Zn$_2$AlCu]	2.5	10
[Zn$_2$AlCo]	2.8	10.5
[Zn$_2$AlMn]	3.3	10.7
[Zn$_2$AlGa]	2.5	10

efficient when mesopores and micropores are present in a same compound. So, for this BJH study, we could only compare the behaviors of the different compounds studied in this paper and reasonably suppose that the mesoporous nature is surely preserved after calcination, even if observed microporosity increased for all studied compounds.

Aggregate sizes were measured by laser diffraction particles sizing on noncalcined compounds; the results are reported in Table 14. A double distribution in aggregates size appeared, which seems to be controlled by the nature of the intercalated anion. The observed sizes indicate that LDH particles are aggregated, which could explain the low values of BET surface areas for non-calcined phases.

To obtain more dispersed metallic oxides in the midst of amorphous phases, we used for intercalated LDH compounds a polyol treatment which was previously described for zeolite materials.[61−64] In this aim, we realized an adapted treatment: maintaining the compounds under refluxing ethylene glycol during three weeks under nitrogen atmosphere with poly(vinylpyrrolidone) as catalyst. The resulting products showed small and broad diffraction lines characteristic of dispersed and poorly crystallized oxides and copper metal (Figure 10).

For other compounds related in this paper, we did not observe crystallized metallic particles dispersed on amorphous phases as for metallic platinum com-

(59) Malherbe, F.; Forano, C.; Besse, J. P. *Microporous Mater.* **1997**, *10*, 67.
(60) Groen, J. C.; Peffer, L. A. A.; Pérez-Ramirez, J. *Microporous Mesoporous Mater.* **2003**, *60*, 1.
(61) Figlarz, M.; Fiévet, F.; Lagier, J. P. Brevet France no. 821483, Europe no. 0113281, U.S. no. 4539041, Finlande no. 74416.
(62) Fiévet, F.; Lagier, J. P.; Beaudoin, B.; Figlarz, M.; Barret, P.; Dufour, L. C., Eds.; Elsevier: Amsterdam, 1985; p 555.
(63) Hedge, M. S.; Larcher, D.; Dupont, L.; Beaudoin, B.; Tekaia-Elhsissen, K.; Tarascon, J. M. *Solid State Ionics* **1997**, *93*, 33.
(64) Jacobs, P. A.; Tielsen, M.; Linart, J. P.; Uytterhoeven, J. B. *J. Chem. Soc., Faraday Trans. 1* **1976**, *72*, 2793.
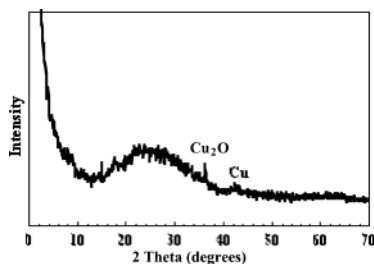
Figure 10. Diffraction patterns of [Zn$_2$AlCu] treated in ethylene glycol.

plexes.[41] So it seems that, generally, only dispersed oxides could be obtained with this method using LDH intercalated by metallic oxalato complexes as starting materials.

4. Conclusion

This work has evidenced that metallic oxalato complexes can be intercalated into [Zn$_2$Al] and [Mg$_2$Al] LDHs with minor structural modifications following a new intercalation process. A structural study described the interlamellar domain. Interactions between layers and complexes exist but are not strong enough to modify the complexes structure. It is not usual that metals such as Co, Cu, Mn, and Ga are located in the LDH interlamellar domain rather than in the layers. As thermal treatments carried out on these compounds lead to metals oxides mixtures, one can expect a better dispersion of metallic species in the midst of obtained powder compared to that of catalysts prepared by impregnation. So interesting perspectives of this work could first consist of comparative catalytic tests carried out on catalysts prepared from LDHs compounds containing the same metal either impregnated, or structurally located, in the host lattice either in the layers or in the interlamellar domain. Second, the preservation of metallic complexes structure between layers could offer new possibilities for metallic complexes intercalation, in which ligands would choose to develop, after thermal treatments, basic or acidic catalytic sites.